Fuel 181 (2016) 358–365

Contents lists available at ScienceDirect

Fuel

journal homepage: www.elsevier.com/locate/fuel

Full Length Article

Ammonia oxidation at high pressure and intermediate temperatures

Yu Song [a,b], Hamid Hashemi [a], Jakob Munkholt Christensen [a], Chun Zou [b], Paul Marshall [c], Peter Glarborg [a,*]

[a] Department of Chemical and Biochemical Engineering, Technical University of Denmark, DK-2800 Kgs. Lyngby, Denmark
[b] State Key Laboratory of Coal Combustion, Huazhong University of Science and Technology, Wuhan 430074, China
[c] Department of Chemistry and Center for Advanced Scientific Computing and Modeling (CASCaM), University of North Texas, 1155 Union Circle #305070, Denton, TX 76203-5017, United States

ARTICLE INFO

Article history:
Received 11 January 2016
Received in revised form 9 March 2016
Accepted 21 April 2016
Available online 10 May 2016

Keywords:
NH_3 oxidation
High pressure
Flow reactor
$H_2NO + O_2$ rate constant
Kinetic model

ABSTRACT

Ammonia oxidation experiments were conducted at high pressure (30 bar and 100 bar) under oxidizing and stoichiometric conditions, respectively, and temperatures ranging from 450 to 925 K. The oxidation of ammonia was slow under stoichiometric conditions in the temperature range investigated. Under oxidizing conditions the onset temperature for reaction was 850–875 K at 30 bar, while at 100 bar it was about 800 K, with complete consumption of NH_3 at 875 K. The products of reaction were N_2 and N_2O, while NO and NO_2 concentrations were below the detection limit even under oxidizing conditions. The data were interpreted in terms of a detailed chemical kinetic model. The rate constant for the reaction of the important intermediate H_2NO with O_2 was determined from ab initio calculations to be $2.3 \times 10^2\, T^{2.994} \exp(-9510\ K/T)\ cm^3\ mol^{-1}\ s^{-1}$. The agreement between experimental results and model work was satisfactory. The main oxidation path for NH_3 at high pressure under oxidizing conditions is $NH_3 \xrightarrow{+OH} NH_2 \xrightarrow{+HO_2,NO_2} H_2NO \xrightarrow{+O_2} HNO \xrightarrow{+O_2} NO \xrightarrow{+NH_2} N_2$. The modeling predictions are most sensitive to the reactions $NH_2 + NO = NNH + OH$ and $NH_2 + HO_2 = H_2NO + OH$, which promote the ammonia consumption by forming OH radicals, and to $NH_2 + NO = N_2 + H_2O$ and $NH_2 + NO_2 = N_2O + H_2O$, which are the main chain-terminating steps.

1. Introduction

Ammonia is an important combustion intermediate in formation of nitric oxide from nitrogen organically bound in fuels. For most solid fuels, NH_3 is formed directly during devolatilization [1], and it has also been reported as a product of gasification [2]. The selectivity for forming NO or N_2 from N-volatiles in combustion depends largely on the fate of amine radicals such as NH_2, NH, and N [1,3]. Ammonia is also known as an efficient additive for Selective Non-Catalytic Reduction of NO (SNCR) [3,4]. Recently, ammonia has attracted interest as a potential carbon-free energy carrier [5]. Results on oxidation of NH_3 are available from flames [6–16], shock tubes [17–27], and flow reactors [2,28–30]. In addition, a number of modeling studies and reviews of ammonia chemistry have been reported [3,27,28,31–35]. Supplementing the oxidation studies, extensive work has been conducted on the kinetics of the SNCR process [3,4,36–38].

With the interest in amine-based fuels as energy carriers [39], reliable experimental data for oxidation of ammonia at high pressure become important. High-temperature results at increased pressure are available from recent work in shock tubes and premixed flames. Mathieu and Petersen [27] measured the ignition time for ammonia diluted in Ar at 1.4, 11, and 30 bar, respectively, while Hayakawa et al. [15] determined the burning velocity of ammonia/air mixtures at pressures of 1–5 bar. However, studies of ammonia oxidation at low-to-medium temperatures and high pressure are scarce.

The purpose of the present study is to investigate ammonia oxidation at high pressure (30–100 bar) and temperatures up to 925 K. Experiments are conducted with stoichiometric and lean NH_3/O_2 mixtures, highly diluted in N_2, in a laminar flow reactor. The results are interpreted in terms of a detailed chemical kinetic model for ammonia oxidation. The reaction mechanism, which is based on earlier work on nitrogen chemistry [34,38,40,41], is updated in the present work, emphasizing reactions important at high pressure. Under the present conditions, the nitroxide radical H_2NO is an important intermediate, and the rate constant for the

* Corresponding author.
E-mail address: pgl@kt.dtu.dk (P. Glarborg).

http://dx.doi.org/10.1016/j.fuel.2016.04.100
0016-2361/

reaction between H_2NO and O_2 has been derived from ab initio calculations.

2. Experimental

The experimental setup was a laboratory-scale high-pressure laminar flow reactor designed to approximate plug flow. The setup is described in detail elsewhere [42] and only a brief description is provided here. The system was used here for investigation of ammonia oxidation at 30 bar and 100 bar pressure, respectively, and temperatures from 450 to 925 K. The reactant gases were premixed before entering the reactor. The reactions took place in a tube under laminar flow conditions. The tube was made of quartz (inner diameter of 7.5 mm) or alumina (Degussit AL23, inner diameter 6 mm). The temperature profile in the flow reactor was measured by a thermocouple positioned in the void between the quartz reactor and the steel shell. Results for 100 bar are shown in Fig. 1 while the 30 bar profiles are available as supplementary material. An isothermal reaction zone of 39–47 cm was achieved in the reactor. All gases used in the present experiments were high purity gases or mixtures with certified concentrations. The total flow rate was 2.8 L min^{-1} (STP). The product analysis was conducted with an on-line 6890N Agilent Gas Chromatograph (GC-TCD/FID from Agilent Technologies) and an AO2020 NH_3/NO/NO_2 analyser from ABB. The relative measurement uncertainties for the species detected were in the range ±2–6%.

3. Chemical kinetic model

The starting mechanism and corresponding thermodynamic properties were drawn from the recent work by Klippenstein et al. [38]. The mechanism was carefully updated, emphasizing reactions of importance under the conditions of the present study. Table 1 lists the key reactions in the NH_3 oxidation scheme with the rate coefficients used in the present work. The full mechanism is available as supplemental material.

At the high-pressure medium-temperature conditions of this work, ammonia oxidation occurs to a significant extent through the H_2NO intermediate. Rate constants for H_2NO reactions are generally quite uncertain. In the present work, we characterize the key reaction of H_2NO with O_2 by ab initio calculations, as described below.

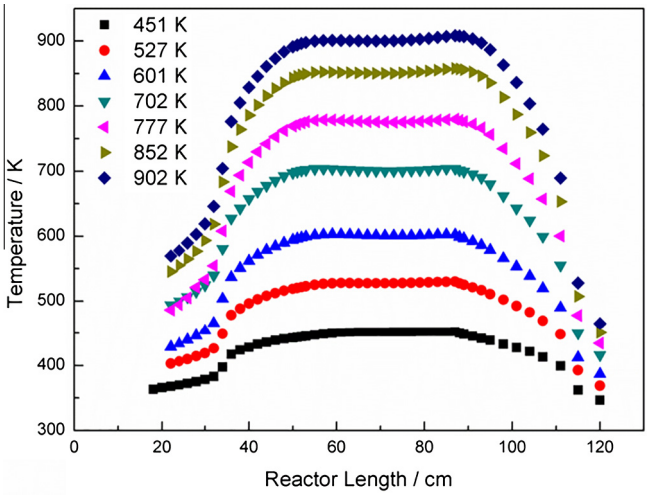

Fig. 1. Measured temperature profiles along the reactor axis for 100 bar conditions.

Table 1
Selected reactions from the NH_3 subset. Parameters for use in the modified Arrhenius expression $k = AT^{\beta} \exp(-E/[RT])$. Units are mol, cm, s, cal.

		A	β	E	Source
1	$NH_2 + H(+M) \rightleftharpoons NH_3(+M)$	1.6E14	0.000	0	[43]
	Low pressure limit:	3.6E22	−1.760	0	
	Troe parameters: 0.5 1.0E−30 1.0E30				
2	$NH_3 + H \rightleftharpoons NH_2 + H_2$	6.4E05	2.390	10,171	[44]
3	$NH_3 + O \rightleftharpoons NH_2 + OH$	9.4E06	1.940	6460	[45]
4	$NH_3 + OH \rightleftharpoons NH_2 + H_2O$	2.0E06	2.040	566	[46]
5	$NH_3 + HO_2 \rightleftharpoons NH_2 + H_2O_2$	3.0E11	0.000	22,000	[3] est
6	$NH_2 + HO_2 \rightleftharpoons NH_3 + O_2$	1.7E04	1.550	2027	[47][a]
7	$NH_2 + H \rightleftharpoons NH_2 + H_2$	7.2E05	2.320	799	[48]
8	$NH_2 + O \rightleftharpoons HNO + H$	6.6E13	0.000	0	See [41]
9	$NH_2 + O \rightleftharpoons NH + OH$	7.0E12	0.000	0	See [41]
		8.6E−1	4.010	1673	
10	$NH_2 + OH \rightleftharpoons NH + H_2O$	3.3E06	1.949	−217	[38,49]
11	$NH2 + HO_2 \rightleftharpoons H_2NO + OH$	5.0E13	0.000	0	See text
12	$NH_2 + HO_2 \rightleftharpoons HNO + H_2O$	1.6E07	0.550	525	[47][a,b]
		5.7E15	−1.120	707	
13	$NH_2 + HO_2 \rightleftharpoons HON + H_2O$	2.1E07	0.640	811	[47][a]
14	$NH_2 + O_2 \rightleftharpoons H_2NO + O$	2.6E11	0.487	29,050	[38]
15	$NH_2 + O_2 \rightleftharpoons HNO + OH$	2.9E−2	3.764	18,185	[38]
16	$NH_2 + NH_2 \rightleftharpoons NH_3 + NH$	5.6E00	3.530	552	[49]
17	$NH_2 + HNO \rightleftharpoons NH_3 + NO$	3.6E06	1.630	−1250	[50]
18	$NH_2 + NO \rightleftharpoons N_2 + H_2O$	1.3E16	−1.25	0	[38]
		−3.1E13	−0.48	1180	
19	$NH_2 + NO \rightleftharpoons NNH + OH$	3.1E13	−0.48	1180	[38]
20	$NH_2 + NO_2 \rightleftharpoons N_2O + H_2O$	2.6E18	−2.191	455	[51]
21	$NH_2 + NO_2 \rightleftharpoons H_2NO + NO$	9.1E11	0.032	−1512	[51]
22	$NH_2 + HONO \rightleftharpoons NH_3 + NO_2$	7.1E01	3.020	−4940	[50]
23	$H_2NO + M \rightleftharpoons HNO + H + M$	2.8E24	−2.830	64,915	[33]
24	$H_2NO + H \rightleftharpoons HNO + H_2$	3.0E07	2.000	2000	[36] est
25	$H_2NO + H \rightleftharpoons NH_2 + OH$	5.0E13	0.000	0	[36] est
26	$H_2NO + O \rightleftharpoons HNO + OH$	3.0E07	2.000	2000	[36] est
27	$H_2NO + OH \rightleftharpoons HNO + H_2O$	1.0E14	0.000	0	[52]
28	$H_2NO + HO_2 \rightleftharpoons HNO + H_2O_2$	2.9E04	2.690	−1600	[33]
29	$H_2NO + O_2 \rightleftharpoons HNO + HO_2$	2.3E02	2.994	18,900	pw
30	$H_2NO + NH_2 \rightleftharpoons HNO + NH_3$	3.0E12	0.000	1000	[36] est
31	$H_2NO + NO_2 \rightleftharpoons HONO + HNO$	6.0E11	0.000	2000	[53] est
32	$HNO + O_2 \rightleftharpoons NO + HO_2$	2.0E13	0.000	16,000	[33]
33	$NNH \rightleftharpoons N_2 + H$	1.0E09	0.000	0	[38]
34	$NNH + O_2 \rightleftharpoons N_2 + HO_2$	5.6E14	−0.385	−13	[38]

[a] Rate constant calculated for 1 atm.
[b] Duplicate reaction – the resulting rate constant is the sum of the two expressions.

3.1. Ab initio calculations

The nitroxide radical H_2NO, molecular oxygen and the transition state for their reaction were investigated computationally. First, geometries and frequencies (scaled by a standard factor of 0.954 [54]) were obtained with UQCISD/6-311G(d,p) theory, using spin-unrestricted wavefunctions as implemented within the Gaussian 09 code [55]. At these geometries (see Fig. 2), single-point energies were calculated at the UCCSD(T) level of theory with the aug-cc-pVTZ and aug-cc-pVQZ basis sets, using spin-restricted wavefunctions within the Molpro 2010 program [56], and extrapolated to the complete basis set limit for coupled cluster theory (CCSD(T)/CBS). Corrections were added to this result based on UCCSD(T)/cc-pwVTZ results obtained with core electrons included and excluded from the correlation treatment, and relativistic effects evaluated at the CISD/cc-pwVTZ level of theory. The results are summarized in the supplementary material. The rate constant was then derived via canonical transition state theory as implemented within the Multiwell program suite [57], with tunneling accounted for via the Eckart model.

Some of the prior studies of H_2NO raised the issue of whether this molecule is planar or pyramidal [58,59]. Out-of-plane bending

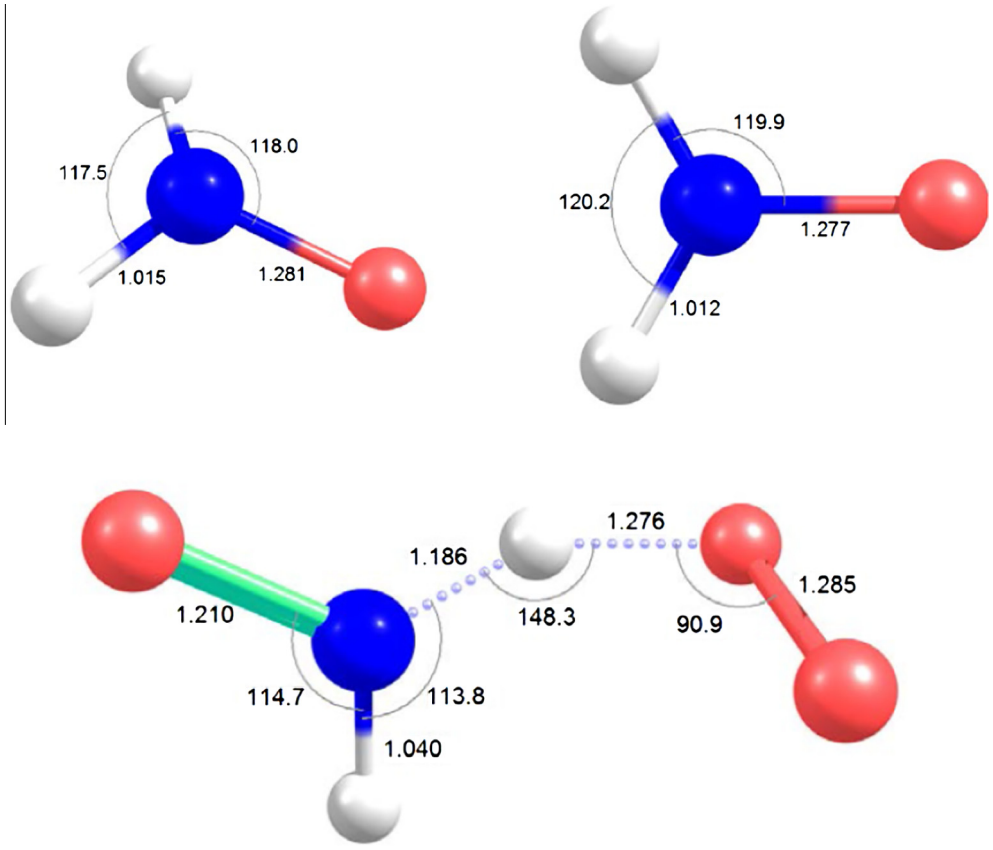

Fig. 2. UQCISD/6-311G(d,p) geometries of $^2A'$ H_2NO, the planar $^2B_1$ barrier to inversion, and the transition state for abstraction of H by O_2. Distances are in Å and angles in degrees. Dihedral angles in the TS: HNHO −159.2°, OHNH −49.2°, OOHN −24.2°.

of the C_{2V} structure was explored via scans of the angle between the O–N bond and the NH_2 plane, with the rest of the geometry allowed to optimize. The results are plotted in Fig. 3 that shows a double well potential with a very small barrier of 17 cm^{-1} to inversion. The harmonic frequency evaluated at either minimum is 481 cm^{-1}, but clearly the potential is significantly anharmonic.

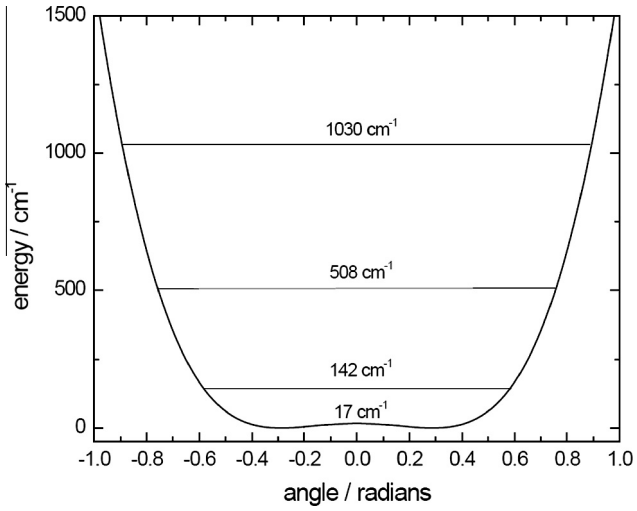

Fig. 3. The double-well potential of H_2NO computed at the UQCISD/6-311G(d,p) level of theory. The barrier height and the first three eigenvalues for out-of-plane bending are relative to the minima. The angle is defined as the deviation from 180° (the planar conformation) for the angle O–N–X where X is a point midway between the two H atoms.

The moment of inertia for bending was estimated to be 0.407 amu $Å^2$, by treating the planar geometry like a three-atom linear molecule [60] with a mass of 2 amu at the midpoint of the two H atoms. The eigenvalues obtained via the FGH method [61] for quantized bending motion on this potential are summarized in the supplemental material; the first three are 142, 508 and 1030 cm^{-1} above the minima. Even the lowest level is well above the inversion barrier so H_2NO explores both sides equally. Because the wavefunction for the ground state is maximized at the planar geometry, we use this structure and a symmetry number of 2 to calculate rotational partition functions. Vibrational partitions were based on the harmonic oscillator model for the remaining 5 modes of H_2NO combined with results derived via a direct count for the out-of-plane bending energy levels. Together with the heat of formation at 298 K from the Active Thermochemical Tables [62], the thermochemistry is summarized within the NASA polynomial included in the supplemental information.

3.2. Reaction mechanism

The reactions of ammonia with the radical pool and O_2 involve hydrogen abstraction to form NH_2. The rate constants for these steps, taken from the mechanism of Klippenstein et al. [38], are mostly well established, but the values for $NH_3 + HO_2$ (R4) (estimated [3]) and $NH_3 + O_2$ (R5b) (ab initio calculation [47]) are more uncertain.

The oxidation rate for ammonia and the products of reaction are largely determined by the fate of NH_2. The NH_2 radical is mainly consumed by reaction with the HO_2 radical (R5b, R11–R13), which builds up in considerable concentrations under the present conditions, and with the stable species NO (R18, R19) and NO_2 (R20,

R21). The $NH_2 + HO_2$ reaction has been studied theoretically by several groups [33,47,63–65], while there are only indirect room temperature measurements available for the rate constant [66–68]. It has a number of product channels and may occur both on the singlet and triplet surfaces. We choose to rely on the work of Sumathi and Peyerimhoff [47] who calculated rate constants for formation of the adduct H_2NOOH and its isomers HN(OH) OH and $H_2N(OH)$ O, as well as the products $NH_3 + O_2$, $NH_2O + OH$, $HNO + H_2O$, and $HON + H_2O$. The predominant contribution to the total rate constant is predicted to be dissociation of energized H_2NOOH to $NH_2O + OH$ over the temperature range 300–2000 K and pressures from 0.001 to 10 atm. At pressures above 10 atm, stabilisation of H_2NOOH becomes important according to Sumathi and Peyerimhoff. However, little is known about the fate of the H_2NOOH adduct. In the present work, we take $H_2NO + OH$ (R11) to be the primary products of reaction and assume the rate constant to be equal to the high-pressure limit of the overall reaction, which we estimate to be 5×10^{13} cm^3 mol^{-1} s^{-1}. This value is only slightly higher than the indirect measurement for $NH_2 + HO_2$ by Lozovskii et al. [67] at 570 torr, but a factor of two higher than the calculation of Sumathi and Peyerimhoff.

The rate constants for the reactions of NH_2 with NO and NO_2,

$$NH_2 + NO \rightleftharpoons N_2 + H_2O \quad (R18)$$

$$NH_2 + NO \rightleftharpoons NNH + OH \quad (R19)$$

$$NH_2 + NO_2 \rightleftharpoons N_2O + H_2O \quad (R20)$$

$$NH_2 + NO_2 \rightleftharpoons H_2NO + NO \quad (R21)$$

have been discussed in detail in recent work by Klippenstein and coworkers [38,51]. We have adopted their values without modifications. For $NH_2 + NO_2$, formation of the adducts H_2NNO_2 and H_2NONO is pressure dependent, but Klippenstein et al. predict little effect of pressure below 100 atm because the complex lifetimes are too short to permit significant collisional relaxation [51].

Nitroxide may be formed in significant quantities from reaction of NH_2 with HO_2 and NO_2. The H_2NO subset of the reaction mechanism consists largely of reactions with estimated rate constants. While the most important reaction of H_2NO is that with O_2, discussed above, also the reactions with HO_2 (R28) and NH_2 (R30) are important consumption steps. The value of k_{28} is a rough estimate [36] and k_{30} was derived from QRRK calculations [33]. Similarly to H_2NO, HNO is mostly consumed by reaction with O_2 (R32); also for this step we use a rate constant based on QRRK theory [33].

4. Results and discussion

Experiments for NH_3 oxidation with high dilution in N_2 as a function of temperature from 450 K to 900 K were conducted under stoichiometric and oxidizing conditions. Table 2 lists the experimental conditions. The fuel–air equivalence ratio, defined from the overall reaction $NH_3 + 1.25O_2 \rightarrow NO + 1.5H_2O$, ranged from approximately 1.0 to 0.02. Simulations with the full temperature profile were conducted using the CHEMKIN PRO software package [69]. Calculations restricted to the isothermal zone of the reactor showed similar trends, but with a smaller conversion at the highest temperatures (oxidizing conditions). The experimental results are compared with modeling predictions in Figs. 4–7. Symbols denote the experimental data and lines denote numerical results.

Figs. 4 and 5 show results for NH_3 oxidation under stoichiometric conditions and pressures of 30 and 100 bar, respectively. At 30 bar the onset of reaction occurs at 800 K. However, even above this temperature consumption of NH_3 is very slow; at 925 K 730 ppm NH_3 (95% of the inlet concentration) and about 900 ppm O_2 (97% of the inlet concentration) are still unreacted in the reactor outlet. At 100 bar, NH_3 consumption also starts around 800 K, but as the temperature increases oxidation is slightly faster than at 30 bar. This can partly be attributed to a longer residence time. However, at 900 K still 675 ppm NH_3 (i.e., 95% of the inlet) remains unreacted.

The modeling results for stoichiometric conditions at 30 bar and 100 bar show very little reaction. The agreement with experiment can be considered satisfactory, since the measurements show that only around 40 ppm or about 5% of NH_3 are consumed at the highest temperatures at the two pressures.

Fig. 6 shows the results for NH_3 oxidation at 30 bar for fuel-lean conditions. To investigate the impact of surface effects, these experiments were conducted in both an alumina and a quartz tube. Ammonia is known to decompose on quartz surfaces [70–72], and while surface effects are unimportant in SNCR for experiments carried out at low surface-to-volume ratios [36,73], it has been observed that induction times for oxidation of NH_3 in quartz reactors were influenced by heterogeneous effects [28].

In the figure, the closed symbols indicate experimental results obtained in the quartz tube, while the open symbols denote results from the alumina tube. In the quartz tube, the onset temperature for reaction occurs at 850 K, compared to a value of 875 K observed in the alumina tube. The difference can partly be attributed to the longer residence time in the quartz reactor, but it cannot be ruled out that some surface initiation takes place in the quartz reactor, despite the high pressure.

Upon initiation, NH_3 is oxidized to N_2 (not quantified) and N_2O; the concentrations of NO and NO_2 in the product gas were below detection limit. Nitrous oxide is formed in significant amounts, reaching 50 ppm in the alumina reactor and levels above 100 ppm in the quartz reactor at 900 K.

At 100 bar (Fig. 7), reaction is initiated already at 800–825 K, partly due to the longer residence time, and NH_3 is fully oxidized at 875–900 K. The N_2O concentration approaches 200 ppm, corresponding to a selectivity for forming N_2O from NH_3 of about 50%. The N_2O profiles from the quartz and alumina reactors indicate a difference in onset temperature, but the peak concentrations are similar.

Table 2
Experimental conditions for the NH_3 oxidation study.

Experiment	Inlet composition[a]	Pressure (bar)	Temperature (K)	Residence time[b] (s)	Reactor
1	772 ppm NH_3, 929 ppm O_2 (ϕ = 1.04)	30	450–925	3100/T[K]	Quartz
2	714 ppm NH_3, 864 ppm O_2 (ϕ = 1.03)	100	450–925	10,330/T[K]	Quartz
3	729 ppm NH_3, 3.95%(v) O_2 (ϕ = 0.23)	30	450–925	3100/T[K]	Quartz
4	719 ppm NH_3, 4.03%(v) O_2 (ϕ = 0.22)	30	450–925	1984/T[K]	Alumina
5	789 ppm NH_3, 4.07%(v) O_2 (ϕ = 0.24)	100	450–925	10,330/T[K]	Quartz
6	789 ppm NH_3, 4.07%(v) O_2 (ϕ = 0.24)	100	450–925	6610/T[K]	Alumina

[a] Volume basis; balance N_2.
[b] The nominal residence time in the isothermal region of the reactor. It is a function of temperature, since the mass flow rate was held constant.

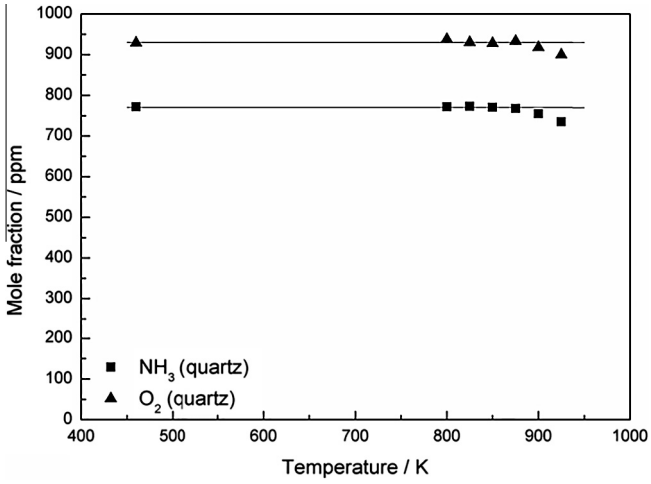

Fig. 4. Comparison of experimental and predicted concentration profiles as a function of the reactor temperature for the stoichiometric experiment at 30 bar in the quartz reactor. The symbols mark experimental data while solid lines denote model predictions obtained at isothermal conditions. Inlet composition: 772 ppm NH_3, 929 ppm O_2; balance N_2. The fuel–air equivalence ratio is $\phi = 1.04$ and the residence time in the isothermal zone is calculated from $\tau[s] = 3100/T[K]$.

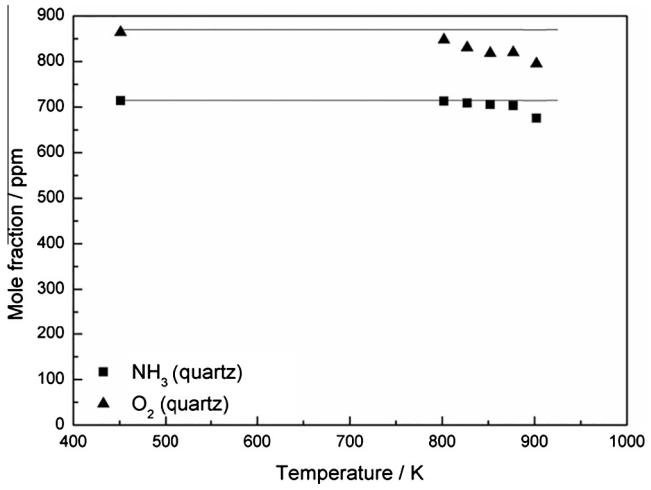

Fig. 5. Comparison of experimental and predicted concentration profiles as a function of the reactor temperature for the stoichiometric experiment at 100 bar in the quartz reactor. The symbols mark experimental data while solid lines denote model predictions obtained at isothermal conditions. Inlet composition: 714 ppm NH_3, 864 ppm O_2; balance N_2. The fuel–air equivalence ratio is $\phi = 1.03$ and the residence time in the isothermal zone is calculated from $\tau[s] = 10{,}330/T[K]$.

The model satisfactorily predicts the experimental data. The best agreement is obtained for the alumina reactor data, which are possibly more reliable. At 30 bar, the agreement is very good, while at 100 bar the temperature for onset of reaction is slightly overpredicted. The most important difference is that the concentration of N_2O is underpredicted at the highest pressure. In line with observations, the model predicts that any NO or NO_2 formed are rapidly consumed.

Fig. 8 shows the results of a rate of production analysis under oxidizing conditions. The arrow thickness distinguishes the main and minor routes for ammonia consumption. Results are shown for 100 bar conditions, but the reaction paths are similar for 30 bar. The main oxidation for ammonia is $NH_3 \xrightarrow{+OH} NH_2 \xrightarrow{+HO_2,NO_2} H_2NO \xrightarrow{+O_2} HNO \xrightarrow{+O_2} NO \xrightarrow{+NH_2} N_2$. Ammonia is mainly consumed through the reaction $NH_3 + OH = NH_2 + H_2O$ (R4). The

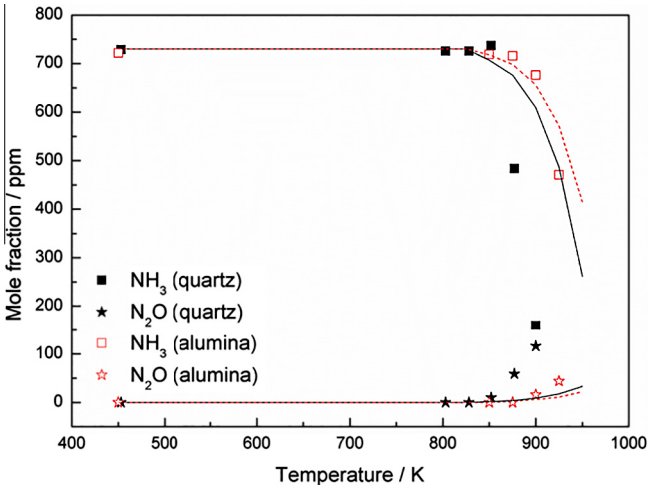

Fig. 6. Comparison of experimental and predicted concentration profiles as a function of the reactor temperature for the oxidizing experiment at 30 bar, obtained in a quartz and alumina tube, respectively. The symbols mark experimental data while solid lines denote model predictions obtained at isothermal conditions. Inlet composition: 729 ppm NH_3, 3.95%(v) O_2; balance N_2. The fuel–air equivalence ratio is $\phi = 0.023$ and the residence time in the isothermal zone is calculated from $\tau[s] = 3100/T[K]$ for the quartz tube and $\tau[s] = 1984/T[K]$ for the alumina tube.

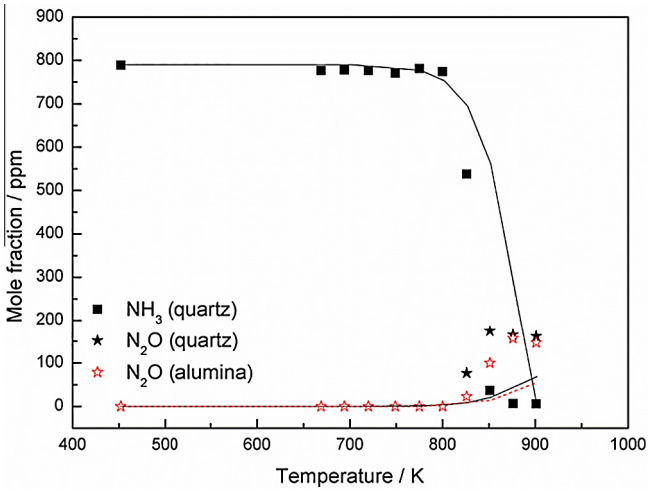

Fig. 7. Comparison of experimental and predicted concentration profiles as a function of the reactor temperature for the oxidizing experiment at 100 bar, obtained in a quartz and alumina tube, respectively. The symbols mark experimental data while solid lines denote model predictions obtained at isothermal conditions. Inlet composition: 789 ppm NH_3, 4.07%(v) O_2; balance N_2. The fuel–air equivalence ratio is $\phi = 0.024$ and the residence time in the isothermal zone is calculated from $\tau[s] = 10{,}330/T[K]$ for the quartz tube and $\tau[s] = 6610/T[K]$ for the alumina tube.

peroxide radical HO_2 is the main chain carrier under the present conditions with high pressure and low to intermediate temperatures. However, HO_2 is partly converted to OH through the fast steps,

$$NO + HO_2 \rightleftharpoons NO_2 + OH$$

$$NH_2 + HO_2 \rightleftharpoons H_2NO + OH \quad (R11)$$

In addition to (R11), the NH_2 radical reacts mainly with NO_2,

$$NH_2 + NO_2 \rightleftharpoons N_2O + H_2O \quad (R20)$$

$$NH_2 + NO_2 \rightleftharpoons H_2NO + NO \quad (R21)$$

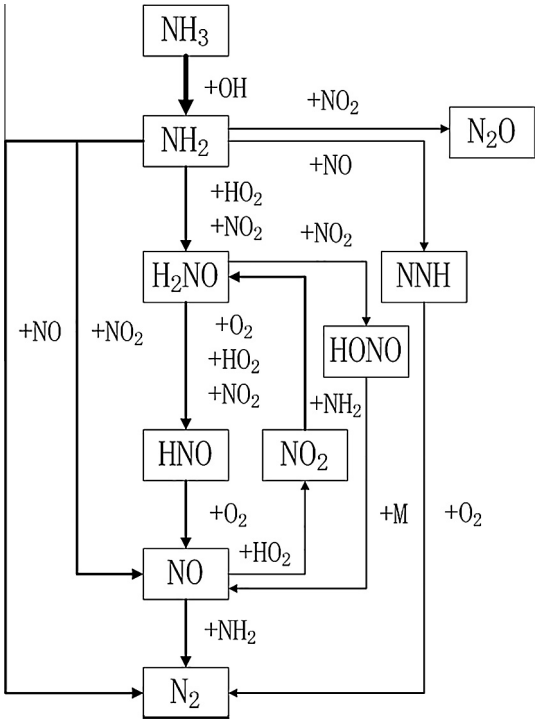

Fig. 8. Main reaction pathways for NH_3 oxidation at the investigated conditions. The diagram is based on the 100 bar oxidizing condition at a temperature of 875 K, but reaction paths are similar at 30 bar oxidizing conditions.

Most of the NH_2 is converted to H_2NO (R11, R21). Nitroxide then reacts with O_2 (R29), HO_2 (R28), and NO_2 (R31); these steps all abstract a hydrogen atom from H_2NO to form HNO, which is converted to NO by reaction with O_2 (R32).

$$H_2NO + O_2 \rightleftharpoons HNO + HO_2 \quad (R29)$$

$$H_2NO + HO_2 \rightleftharpoons HNO + H_2O_2 \quad (R28)$$

$$H_2NO + NO_2 \rightleftharpoons HNO + HONO \quad (R31)$$

$$HNO + O_2 \rightleftharpoons NO + HO_2 \quad (R32)$$

Finally, NO reacts with HO_2 or NH_2. The NH_2 + NO reaction leads to formation of N_2, either directly

$$NH_2 + NO \rightleftharpoons N_2 + H_2O \quad (R18)$$

or via

$$NH_2 + NO \rightleftharpoons NNH + OH \quad (R19)$$

followed by rapid dissociation of NNH (R33) or reaction with O_2 (R34).

The reaction $NH_2 + NO_2 = N_2O + H_2O$ (R20) is the main source of N_2O at both 30 bar and 100 bar oxidizing conditions. A minor route for consumption of NH_2 is the recombination reaction to form hydrazine,

$$NH_2 + NH_2(+M) \rightleftharpoons N_2H_4(+M)$$

Fig. 9 shows the results of a sensitivity analysis for oxidizing conditions at 30 and 100 bar. The coefficients were obtained by varying A-factors for all reactions by a factor of two. Reactions of NH_2 with NO and NO_2 are important for the oxidation rate. For both reactions a chain propagating/branching product channel,

$$NH_2 + NO \rightleftharpoons NNH + OH \quad (R19)$$

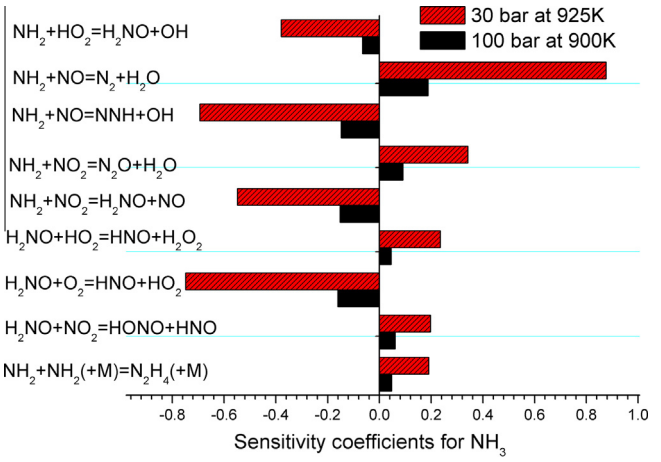

Fig. 9. First order sensitivity coefficients for NH_3 for conditions of 30 bar (925 K) and 100 bar (900 K).

$$NH_2 + NO_2 \rightleftharpoons H_2NO + NO \quad (R21)$$

competes with a chain terminating channel,

$$NH_2 + NO \rightleftharpoons N_2 + H_2O \quad (R18)$$

$$NH_2 + NO_2 \rightleftharpoons N_2O + H_2O \quad (R20)$$

All these steps show up in the sensitivity analysis with large positive (branching) or negative (terminating) coefficients.

Other important reactions which accelerate ammonia consumption are,

$$NH_2 + HO_2 \rightleftharpoons H_2NO + OH \quad (R11)$$

$$H_2NO + O_2 \rightleftharpoons HNO + HO_2 \quad (R29)$$

The reaction $H_2NO + O_2$ (R29) has the largest positive sensitivity coefficients. H_2NO is a significant intermediate species as shown in the reaction path analysis and (R29) is favored by the excess of O_2 in oxidizing conditions. It yields HO_2 radicals, which is converted to the more reactive OH radical by $NH_2 + HO_2$ (R11).

The following chain terminating steps inhibit the ammonia consumption,

$$H_2NO + HO_2 \rightleftharpoons HNO + H_2O_2 \quad (R28)$$

$$H_2NO + NO_2 \rightleftharpoons HONO + HNO \quad (R31)$$

$$NH_2 + NH_2(+M) \rightleftharpoons N_2H_4(+M)$$

Reactions (R28) and (R31) are minor consumption channels for H_2NO, compared to $H_2NO + O_2$ (R29), but sufficiently important to show up in the sensitivity analysis. Similarly, $NH_2 + NH_2(+M)$ is a minor sink for NH_2, but it is strongly chain terminating.

The results show that to develop a reliable reaction mechanism for NH_3 oxidation at the present conditions, it is desirable to obtain more accurate rate constants for several reactions in the H_2NO subset.

5. Conclusions

Ammonia oxidation experiments were conducted at high pressure (30 bar and 100 bar) and temperatures of 450–900 K in oxidizing and stoichiometric conditions. The data were interpreted in terms of a detailed chemical kinetic model, developed for high-pressure conditions. As part of the work, the rate constant for the reaction of $H_2NO + O_2$ was calculated from ab initio theory.

The oxidation of ammonia was slow under stoichiometric conditions in the temperature range investigated. Under oxidizing conditions the onset temperature for reaction was 850–875 K at 30 bar, while at 100 bar it was about 800 K, with complete consumption of NH_3 at 875 K. The products of reaction were N_2 and N_2O, while NO and NO_2 concentrations were below the detection limit even under oxidizing conditions.

The agreement between experimental results and modeling work was satisfactory. The main oxidation path for NH_3 under the present conditions was $NH_3 \xrightarrow{+OH} NH_2 \xrightarrow{+HO_2,NO_2} H_2NO \xrightarrow{+O_2} HNO \xrightarrow{+O_2} NO \xrightarrow{+NH_2} N_2$. The modeling predictions were most sensitive to the reactions $NH_2 + NO = NNH + OH$ and $NH_2 + HO_2 = H_2NO + OH$, which promoted the ammonia consumption by forming OH radicals, and to $NH_2 + NO = N_2 + H_2O$ and $NH_2 + NO_2 = N_2O + H_2O$, which were the main chain-terminating steps.

Acknowledgments

The work is part of the CHEC (Combustion and Harmful Emission Control) research program at DTU Chemical Engineering. YS wishes to acknowledge funding from CSC (China Scholarship Council). PM thanks the R.A. Welch Foundation (Grant B-1174) for support.

Appendix A. Supplementary material

Supplementary data associated with this article can be found, in the online version, at http://dx.doi.org/10.1016/j.fuel.2016.04.100.

References

[1] Glarborg P, Jensen AD, Johnsson JE. Fuel nitrogen conversion in solid fuel fired systems. Prog Energy Combust Sci 2003;29:89–113.
[2] Hasegawa T, Sato M. Study of ammonia removal from coal-gasified fuel. Combust Flame 1998;114:246–58.
[3] Miller JA, Bowman CT. Mechanism and modeling of nitrogen chemistry in combustion. Prog Energy Combust Sci 1989;15:287–338.
[4] Lyon RK. Kinetics and mechanism of thermal DeNOx: a review. In: 194th annu ACS meet; div fuel chem, vol. 32; 1987. p. 433.
[5] Duynslaegher C, Jeanmart H, Vandooren J. Kinetics in ammonia-containing premixed flames and a preliminary investigation of their use as fuel in spark ignition engines. Combust Sci Technol 2009;181:1092–106.
[6] Fenimore CP, Jones GW. Oxidation of ammonia in flames. J Phys Chem 1961;65:298–303.
[7] MacLean DI, Wagner HGg. The structure of the reaction zones of ammonia-oxygen and hydrazine decomposition flames. Proc Combust Inst 1967;11:871–8.
[8] Blint RJ, Dasch CJ. Formation of NO and N_2 from NH_3 in flames. In: ACS symp ser, vol. 249; 1984. p. 87–101.
[9] Dasch CJ, Blint RJ. A mechanistic and experimental study of ammonia flames. Combust Sci Technol 1984;41:223–44.
[10] Dean AM, Chou M-S, Stern D. Nitrogen chemistry in flames. Observations and detailed chemistry. In: ACS symp ser, vol. 249; 1984. p. 71–86.
[11] Dean AM, Chou M-S, Stern D. Kinetics of rich ammonia flames. Int J Chem Kinet 1984;16:633–53.
[12] Zabielsky MF, Seery DJ. High temperature measurements of the rate of the reaction of OH with NH_3. Int J Chem Kinet 1991;17:1191–9.
[13] Bian J, Vandooren J, Van Tiggelen PJ. Experimental study of the structure of an ammonia-oxygen flame. Proc Combust Inst 1988;21:953–63.
[14] Sausa RC, Singh G, Lemire GW, Anderson WR. Molecular beam mass spectrometric and modeling studies of neat and NH_3-doped low-pressure H_2/N_2O/Ar flames: formation and consumption of NO. Proc Combust Inst 1996;26:1043–52.
[15] Hayakawa A, Goto T, Mimoto R, Arakawa Y, Kudo T, Kobayashi H. Laminar burning velocity and Markstein length of ammonia/air premixed flames at various pressures. Fuel 2015;159:98–106.
[16] Brackmann C, Alekseev VA, Zhou B, Nordstrom E, Bengtsson P-E, Li Z, et al. Structure of premixed ammonia + air flames at atmospheric pressure: laser diagnostics and kinetic modeling. Combust Flame 2016;163:370–81.
[17] Takeyama T, Miyama H. Kinetic studies of ammonia oxidation in shock waves. I. The reaction mechanism for the induction period. Bull Chem Soc Jpn 1965;38:1670–4.
[18] Takeyama T, Miyama H. Kinetic studies of ammonia oxidation in shock waves. II. The rate of ammonia consumption. Bull Chem Soc Jpn 1966;39:2352–5.
[19] Takeyama T, Miyama H. A shock-tube study of the ammonia-oxygen reaction. Proc Combust Inst 1967;11:845–52.
[20] Bull DC. A shock tube study of the oxidation of ammonia. Combust Flame 1968;12:603–10.
[21] Miyama H. Kinetic studies of ammonia oxidation in shock waves. IV. Comparison of induction periods for the ignition of NH_3-O_2-N_2 with those for NH_3-O_2-Ar mixtures. Bull Chem Soc Jpn 1968;41:1761–5.
[22] Miyama H. Ignition of ammonia-oxygen mixtures by shock waves. J Chem Phys 1968;48:1421–2.
[23] Bradley JN, Butlin RN, Lewis D. Oxidation of ammonia in shock waves. Trans Faraday Soc 1968;64:71–8.
[24] Drummond LJ. High temperature oxidation of ammonia. Combust Sci Technol 1972;5:175–82.
[25] Fujii N, Miyama H, Koshi M, Asaba T. Kinetics of ammonia oxidation in shock waves. Proc Combust Inst 1981;18:873–83.
[26] Salimian S, Hanson RK, Kruger CH. Ammonia oxidation in shock-heated NH_3-N_2O-Ar mixtures. Combust Flame 1984;56:83–95.
[27] Mathieu O, Petersen EL. Experimental and modeling study on the high-temperature oxidation of ammonia and related NOx chemistry. Combust Flame 2015;162:554–70.
[28] Dean AM, Hardy JE, Lyon RK. Kinetics and mechanism of NH_3 oxidation. Proc Combust Inst 1982;19:97–105.
[29] Hulgaard T, Dam-Johansen K. Homogeneous nitrous oxide formation and destruction under combustion conditions. AIChE J 1993;39:1342–54.
[30] Wargadalam VJ, Loffler G, Winter F, Hofbauer H. Homogeneous formation of NO and N_2O from the oxidation of HCN and NH_3 at 600-1000 °C. Combust Flame 2000;120:465–78.
[31] Miller JA, Smooke MD, Green RM, Kee RJ. Kinetic modeling of the oxidation of ammonia in flames. Combust Sci Technol 1983;34:149–76.
[32] Lindstedt RP, Lockwood FC, Selim MA. A detailed kinetic study of ammonia oxidation. Combust Sci Technol 1995;108:231–54.
[33] Dean AM, Bozzelli JW. Combustion chemistry of nitrogen. In: Gardiner WC, editor. Gas phase combustion chemistry. New York: Springer; 2000 [chapter 2].
[34] Skreiberg Ø, Kilpinen K, Glarborg P. Ammonia chemistry under fuel-rich conditions in a flow reactor. Combust Flame 2004;136:501–8.
[35] Duynslaegher C, Contino F, Vandooren J, Jeanmart H. Modeling of ammonia combustion at low pressure. Combust Flame 2012;159:2799–805.
[36] Glarborg P, Dam-Johansen K, Miller JA, Kee RJ, Coltrin ME. Modeling the thermal DENOx process in flow reactors. Surface effects and nitrous oxide formation. Int J Chem Kinet 1994;26:421–36.
[37] Miller JA, Glarborg P. Modeling the thermal De-NOx process: closing in on a final solution. Int J Chem Kinet 1999;31:757–65.
[38] Klippenstein SJ, Harding LB, Glarborg P, Miller JA. The role of NNH in NO formation and control. Combust Flame 2011;158:774–89.
[39] Grinberg Dana A, Tvil G, Winter L, Shter GE, Grader GS. Pressure effect on the combustion of aqueous urea ammonium nitrate alternative fuel. Fuel 2015;159:500–7.
[40] Mendiara T, Glarborg P. Ammonia chemistry in oxy-fuel combustion of methane. Combust Flame 2009;156:1937–49.
[41] Tian Z, Li Y, Zhang L, Glarborg P, Qi F. An experimental and kinetic modeling study of premixed $NH_3/CH_4/O_2$/Ar flames at low pressure. Combust Flame 2009;156:1413–26.
[42] Rasmussen CL, Hansen J, Marshall P, Glarborg P. Experimental measurements and kinetic modeling of $CO/H_2/O_2/NO_x$ conversion at high pressure. Int J Chem Kinet 2008;40:454–80.
[43] Altinay G, Macdonald RG. Determination of the rate constants for the $NH_2(X^2B_1) + NH_2(X^2B_1)$ and $NH_2(X^2B_1) + H$ recombination reactions in N_2 as a function of temperature and pressure. J Phys Chem A 2015;119:7593–610.
[44] Michael JV, Sutherland JW, Klemm RB. Rate constant for the reaction $H + NH_3$ over the temperature range 750-1777 K. J Phys Chem 1986;90:497.
[45] Sutherland JW, Patterson PM, Klemm RB. Flash photolysis-shock tube kinetic investigation of the reaction of O(3P) atoms with ammonia. J Phys Chem 1990;94:2471–5.
[46] Salimian S, Hanson RK, Kruger CH. High-temperature study of the reactions of O and OH with NH_3. Int J Chem Kinet 1984;16:725.
[47] Sumathi R, Peyerimhoff SD. A quantum statistical analysis of the rate constant for the $HO_2 + NH_2$ reaction. Chem Phys Lett 1996;263:742–8.
[48] Linder DP, Duan X, Page M. Ab initio variational transition state theory calculations for the $H + NH_2 = H_2 + NH$ hydrogen abstraction reaction on the triplet potential energy surface. J Phys Chem 1995;99:11458–63.
[49] Klippenstein SJ, Harding LB, Ruscic B, Sivaramakrishnan R, Srinivasan NK, Su M-C, et al. Thermal decomposition of NH_2OH and subsequent reactions: ab initio transition state theory and reflected shock tube experiments. J Phys Chem A 2009;113:10241–59.
[50] Mebel AM, Diau EWG, Lin MC, Morokuma K. Theoretical rate constants for the $NH_3 + NO_x \rightarrow NH_2 + HNO_x$ (x=1,2) reactions by ab initio MO/VTST calculations. J Phys Chem 1996;100:7517–25.
[51] Klippenstein SJ, Harding LB, Glarborg P, Gao Y, Marshall P. Rate constant and branching fraction for the $NH_2 + NO_2$ reaction. J Phys Chem A 2013;117:9011–22.
[52] Sun F, DeSain JD, Scott G, Hung PY, Thompson RI, Glass GP, et al. Reactions of NH_2 with NO_2 and of OH with NH_2O. J Phys Chem A 2001;105:6121–8.
[53] Glarborg P, Dam-Johansen K, Miller JA. The reaction of ammonia with nitrogen dioxide in a flow reactor: implications for the $NH_2 + NO_2$ reaction. Int J Chem Kinet 1995;27:1207–20.

[54] Johnson III RD. Computational chemistry comparison and benchmark database. Version 17b. National Institute of Standards and Technology. <http://cccbdb.nist.gov> [accessed October, 2015].
[55] Frisch MJ, Trucks GW, Schlegel HB, Scuseria GE, Robb MA, Cheeseman JR, et al. Gaussian 09. Wallingford (CT): Gaussian; 2009.
[56] Werner H-J, Knowles PJ, Knizia G, Manby FR, Schutz M, Celani P, et al. MOLPRO. Version 2010.1; 2010. <http://www.molpro.net>.
[57] Barker JR, Ortiz NF, Preses JM, Lohr LL, Maranzana A, Stimac PJ, et al. MultiWell-2014.1. Ann Arbor (MI): University of Michigan; 2014. <http://aoss-research.engin.umich.edu/multiwell/>.
[58] Mikami H, Saito S, Yamamoto S. The microwave-spectrum of the dihydronitrosyl radical, H_2NO (2B1). J Chem Phys 1991;94:3415–22.
[59] Dixon DA, Francisco JS, Alexeev Y. Thermochemical properties of H_xNO molecules and ions from ab initio electronic structure theory. J Phys Chem A 2006;110:185.
[60] Herzberg G. Infrared and Raman spectra of polyatomic molecules, vol. 2. New York: D. Van Nostrand; 1945. p. 632.
[61] Johnson III RD; 1999. <http://www.nist.gov/mml/csd/informatics_research/fourier_grid_hamiltonian_interface.cfm>.
[62] Ruscic B, Active thermochemical tables. Version 1.112. Argonne National Laboratory. <http://atct.anl.gov> [accessed October, 2015].
[63] Pouchan C, Lam B, Bishop DM. A theoretical study of the reaction between NH_2 and HO_2. J Phys Chem 1987;91:4809–13.
[64] Bozzelli JW, Dean AM. Energized complex quantum Rice-Ramsberger-Kassel analysis on reactions of NH_2 with HO_2, O_2 and O atoms. J Phys Chem 1989;93:1058–65.
[65] Xiang TC, Si HY, Han PL, Ruan Y. Theoretical study on the mechanism of the HO_2 plus NH_2 reaction. Comput Theor Chem 2012;985:67–71.
[66] Cheskis SG, Sarkisov OM. Flash photolysis of ammonia in the presence of oxygen. Chem Phys Lett 1979;62:72.
[67] Lozovskii VA, Nadtochenko VA, Sarkisov OM, Cheskis SG. Study of NH_2 radical recombination by intraresonator laser spectroscopy. Kinet Catal 1979;20:918–22.
[68] Lesclaux R. Reactivity and kinetic properties of the NH_2 radical in the gas-phase. Rev Chem Intermed 1984;5:347.
[69] CHEMKIN PRO version 15131. Reaction Design, San Diego, USA; 2013.
[70] Hinshelwood CN, Burk RE. The thermal decomposition of ammonia upon various surfaces. J Chem Soc 1925;127:1105–17.
[71] Roenigk KF, Jensen KF. Low pressure CVD of silicon nitride. J Electrochem Soc 1987;134:1777–85.
[72] Cooper DA, Ljungstrom EB. Decomposition of NH_3 over quartz sand at 840-960 °C. Energy Fuels 1988;2:716–9.
[73] Suhlmann J, Rotzoll G. The influence of quartz glass surfaces on the reduction of NO with NH_3 at high temperatures. Chem Ing Techn 1992;64:580–1.